Vapor Pressure Isotope Effects in Liquid and Solid Ammonia

Tseng-Ven King, Takao Oi *, Anthony Popowicz **, Karl Heinzinger ***, and Takanobu Ishida

Department of Chemistry, State University of New York at Stony Brook, Stony Brook, NY. 11794-3400, U.S.A.

Z. Naturforsch. **44a**, 359–370 (1989); received January 24, 1989

Dedicated to Professor Jacob Bigeleisen on the occasion of his 70th birthday

The H/D and $^{14}N/^{15}N$ vapor pressure isotope effects in liquid and solid ammonia have been measured at temperatures between 163 K and 243 K. The isotopic vapor pressure data have been fitted to $T \ln (P'/P) = A/T - B$ for the liquid/liquid, liquid/solid and solid/solid ranges of temperature. The triple points are; 195.41 K (45.49 torr) for $^{14}NH_3$, 198.96 K (48.35 torr) for $^{14}ND_3$, and 195.58 K (48.83 torr) for $^{15}NH_3$. The isotopic difference in the vapor pressures of NH_3 and ND_3 at temperatures between 195.41 K and 198.96 K is nearly independent of temperature within the present experimental uncertainty. The phase ratios of the reduced partition function ratios, f_{liq}/f_{gas} and f_{sol}/f_{gas}, deduced from these results are well represented by $T \ln (f_c/f_g) = A/T - B$. Molecular forces in the liquid and solid ammonias are discussed using a simple cell and a 4-molecular unit cell model, respectively. The librational motions in the liquid are almost as highly hindered as they are in the solid, but the directionality of the external forces on nitrogen atoms in liquid ammonia is not as well defined as in the solid.

I. Introduction

Vapor pressure isotope effects (VPIE) in ammonia have been studied by few investigators only [1, 2], although the first measurements of the vapor pressure of trideuteroammonia date as far back as 1933 [3]. Figure 1 summarises existing data on the effects of substituting three deuterium atoms for three protium atoms (H/D-VPIE) and substituting ^{15}N for ^{14}N (14/15-VPIE) in the liquid [4–6] and solid [7] ammonias. Evidently significant discrepancies exist in the H/D-VPIE for the liquid, the H/D-data on the solid contain large uncertainties, no reliable VPIE data are available at temperatures between the triple points of isotopic ammonias, and not much is known about the 14/15-VPIE.

In this paper we report on a set of new experimental results on both H/D- and 14/15-VPIE in the liquid and solid ammonias at temperatures ranging from 163 K to 243 K, obtained by using samples of high chemical and isotopic purity, a high-precision differential manometry, and a cryostat built using Bigeleisen's design [8]. We will then present an analysis of the results in the light of Bigeleisen's theory of isotope effects on the thermodynamic properties of condensed system [9] which, almost three decades after its publication, still provides a solid foundation for isotope effect studies of condensed phases. A simple cell model of Stern, Van Hook and Wolfsberg [10] and a 4-molecule unit cell model have been developed to represent the liquid and solid, respectively.

II. Experimental

The measurements of the vapor pressures and their isotopic differences were carried out in a cryostat of the BBIR design [8] with some modifications as described in one of our earlier papers [11]. The temperature of the isotopic samples contained in separate cavities in a copper block of five-nine purity was controlled with a short-time (ca. 2 hrs) stability which is generally far better than ± 0.001 K and well within

* Permanent address: Department of Chemistry, Sophia University, Chiyoda-ku, Tokyo 102, Japan.
** Permanent address: Rockefeller University, New York, NY 10021-6399, U.S.A.
*** Permanent address: Max-Planck-Institut für Chemie (Otto-Hahn-Institut), Mainz, Federal Republic of Germany.

Reprint requests to Dr. T. Ishida, Department of Chemistry, State University of New York at Stony Brook, Stony Brook, NY 11794-3400, U.S.A.

0932-0784 / 89 / 0500-0359 $ 01.30/0. – Please order a reprint rather than making your own copy.

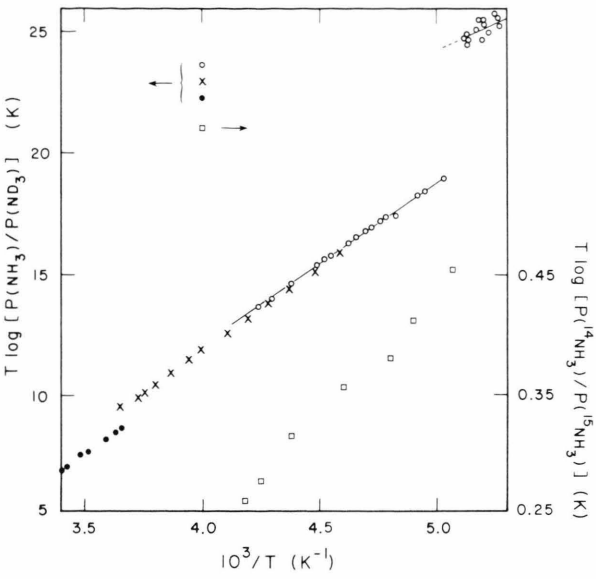

Fig. 1. Summary of previous data on vapor pressure isotope effects in liquid and solid ammonia. *Open circles*; Kirshenbaum and Urey [4] for H/D-VPIE, corrected by Armstrong for 2.1% H in ND_3 sample. *Crosses*; Wolff and Höpfner [5] for H/D-VPIE. *Dark circles*; Groth, Ihle and Murrenhoff [6] for H/D-VPIE. *Squares*; Thode [7] for 14/15-VPIE, corrected for 29.4% ^{14}N in the $^{15}NH_3$ sample. *Lines*; Armstrong [1]. See footnote of Table 2.

± 0.001 K of each other. The stated stability was achieved by detecting fluctuations in the vapor pressure of one of the samples and feeding the information back to a circuit which controls the electric heating of the high heat capacity radiation shields surrounding the copper block. The calibration of the temperature scale has been described earlier [11]. The absolute pressure of ammonia of natural isotopic abundance was measured with a spiral quartz gauge (Mensor Corp. Model No. 10100-001 with sensor No. 10095-001; range $=0-1500$ torr, resolution $=\pm 0.0075$ torr) calibrated with a Ruska dead-weight gauge Model 2460. Measurements of the differences in the isotopic vapor pressures were carried out with a capacitance gauge per isotopic pair (Datametrics Model 572; 0.005% precision in each of the switch-selectable full scale ranges of 100, 30, 10, 3, 0.3 and 0.5 torr).

Samples of isotopic ammonia were purified by the following procedure; (i) bulb-to-bulb distillation, several times, to remove the common impurities (O_2, N_2, CO, CH_4 and other hydrocarbons), (ii) cryogenic distillation over metallic sodium, after liquid ammonia was left standing with sodium for one day, mainly to remove water, and then (iii) a repeated bulb-to-bulb distillation mainly to remove products of reaction with sodium (H_2, CO, CO_2 and CH_4). A new gas chromatographic method had to be developed to determine the part-per-million level of the chemical impurities in ammonia, particularly water. The analytical method may be summarized as follows. A five milliliter (NTP) ammonia sample is injected using a stainless steel sample holder-inlet valve assembly of a special design and eluted through a 10 ft long, 3/16″ I.D., stainless steel column, packed with Porapak R (80/100 mesh) coated with polyethylenimin (10% PEI, M.W. $\approx$ 1000) at 90 °C, with a helium carrier flow rate of about 60 ml NTP/min. It is necessary to have a pressure of about 10 atm at the sample inlet valve in order to maintain this flow rate through the column, an important condition for a satisfactory peak resolution. This procedure yields the detection limits of 5 ppm for water and 3 ppm for all other impurities. Samples of natural abundance ammonia (obtained from Scientific Gas Products, Inc.) and ND_3 and $^{15}NH_3$ (purchased from U.S. Services, Inc.) were purified to at least these detection limits. The purification process described above was repeated until no chemical impurities were detected by the analytical technique. Prevention of re-contamination of ammonia samples by water has been our only most difficult problem throughout the purification, the analytical and other gas-handling processes.

The procedure for the measurement of isotopic vapor pressures in the cryostat has been described in our earlier papers [11–13].

Isotope analysis of the chemically purified ammonia samples was carried out using a Kratos MS30 Dual-beam mass-spectrometer with DS50 database system. The water background was minimized by repeating the process of alternately baking under ultra-high vacuum and saturating the inner walls with purified isotopic ammonia.

III. Results and Discussion

1) Vapor Pressures

Results of 202 measurements of H/D-VPIE and 171 measurements of $^{14}N/^{15}N$-VPIE at temperatures between 163 K and 243 K are plotted in Figs. 2 and 3, respectively. Vapor pressures of the lighter and heavier

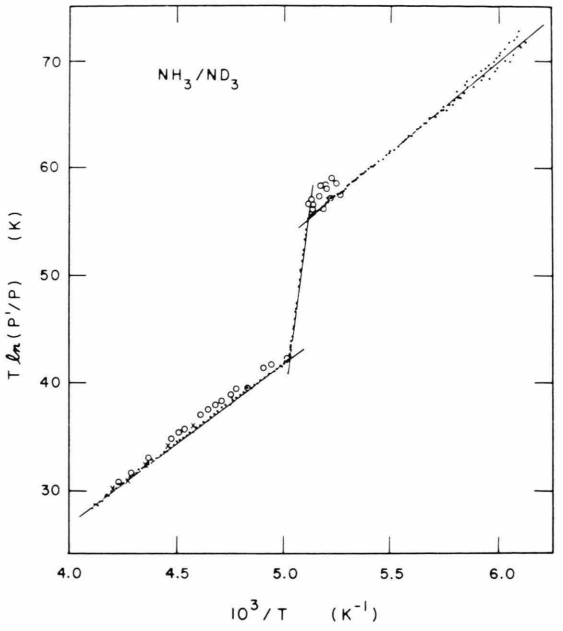

Fig. 2. Observed H/D vapor pressure isotope effects in ammonia. Dots; present work. Circles [4], Crosses [5].

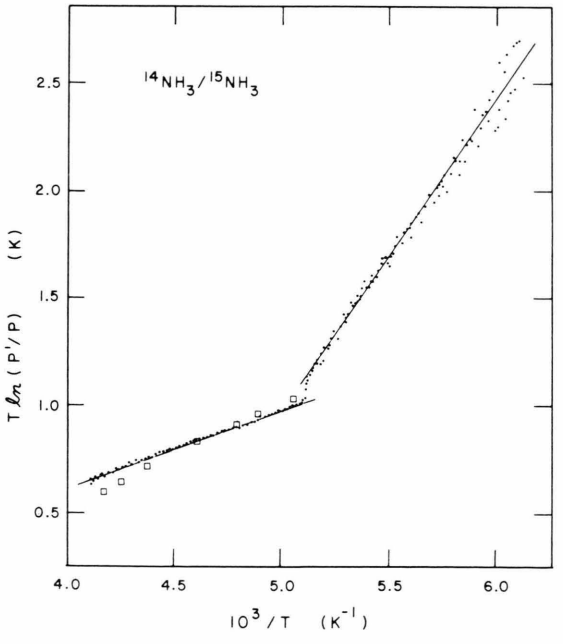

Fig. 3. Observed $^{14}N/^{15}N$ vapor pressure isotope effects in ammonia. Dots; present work. Squares [7].

Table 1. Examples of isotopic differences in the vapor pressures of ammonia (in torrs).

T(K)	P' (NH_3)	δP (NH_3–ND_3)	δP ($^{14}NH_3$–$^{15}NH_3$)
243.01	889.85	98.84	2.444
229.06	431.14	57.01	1.426
219.54	246.87	36.78	0.928
210.96	142.37	23.65	0.600
200.40	66.951	12.657	0.329
198.53	58.058	11.408	0.293
195.36	45.189	11.204	0.258
188.86	23.362	6.259	0.1750
180.02	8.781	2.594	0.0860
168.80	2.196	0.739	0.0301

Table 2. Least-squares fits of isotopic vapor pressure ratios to (1).

Isotopic Pair	Temperature range (K)	A	B	σ
liq d_0/liq d_3	$T_{tr} < T$	15041.2 ±42.9	33.1387 ±0.1976	0.1025
liq d_0/sol d_3	$T'_{tr} < T < T_{tr}$	161084 ±5414	768.112 ±27.426	0.778
sol d_0/sol d_3	$T < T'_{tr}$	16768.7 ± 152.5	29.9744 ±0.8487	0.4715
liq 14/liq 15	$T_{tr} < T$	364.550 ±3.105	0.83480 ±0.01438	0.00795
sol 14/sol 15	$T < T'_{tr}$	1477.21 ±20.90	6.40848 ±0.11658	0.06242

T'_{tr} and T_{tr} are the triple points (cf.: Table 4) of the first- and secondnames isotopic species, respectively. σ is the root mean squares deviation of the present experimental value of $T\ln(P'/P)$ from the least-squares fit line. Armstrong [1] fitted the experimental points of [4] to (1) with following results: $A = 15501$ K and $B = -34.22$ for the liquid; $A = 10393$ K and $B = -4.03$ for the solid.

molecules are denoted by P' and P, respectively. Throughout this paper a primed quantity is the property of the lighter isotopic species of a given pair. The data in Figs. 2 and 3 have been corrected for the presence of 0.36% $^{15}NH_3$ in the normal ammonia sample, 2.7% NHD_2 in trideuteroammonia, and 1.00% $^{14}NH_3$ in the $^{15}NH_3$ sample, using the rule of the geometric means of isotopic compounds [14] and Raoult's law. Table 1 presents examples of experimental points at intervals of roughly 10 K (except around the triple points).

The data are well represented by

$$T\ln(P'/P) = \frac{A}{T} - B. \tag{1}$$

Species	Phase	$\sigma(\log P)$	a	b	c	T(K)	Number of pts
$^{14}NH_3$	Liq	0.00091	9.94326	1471.633	0.0038492	196–243	94
		[0.000167	10.07133	1485.600	0.0041449	199–242	11]
		(0.00123	9.95028	1473.17	0.0038603	196–250	)
	Sol	0.00251	10.01883	1633.785		163–195	109
		[0.000669	10.00528	1630.993		177–195	7]
		(0.00326	9.98379	1627.22		173–195	)
$^{14}ND_3$	Liq	0.00028	10.30672	1541.893	0.0043762	199–243	67
	Sol	0.00289	10.23684	1700.623		163–198	135
$^{15}NH_3$	Liq	0.00060	9.94265	1472.232	0.0038514	196–243	69
	Sol	0.00314	10.04193	1638.775		163–195	102

Table 3. Vapor pressure equations for individual isotopic ammonias: (2) for the liquid, and (3) for the solid.

Values in square brackets are obtained by re-fitting the data of [15] after the ice point correction; see text. Values in parentheses are quoted from [1] in which the data bases were [3, 15, 16a–e] for the liquid and [15, 16a, 16e and 16f] for the solid. All other values are results of the present work.

Table 2 summarizes results of the least-squares fits. The straight lines in Figs. 2 and 3 have been drawn according to (1) and Table 2. Between 202 K and 236 K Kirshenbaum and Urey's data (Fig. 2) are somewhat higher than ours, while Wolff and Höpfner's agree better with ours at the higher liquid temperatures. The very qualitative agreement between Thode's (Fig. 3) and ours is almost fortuitous considering the fact that the points by Thode have been corrected for the presence of 29.4% ^{14}N in his sample.

Vapor pressures of the individual isotopic molecules have been least squares-fitted to the functional form

$$\ln P(\text{torr}) = a - \frac{b}{T(\text{K})} - c\,T(\text{K}) \tag{2}$$

for the liquid and

$$\ln P(\text{torr}) = a - \frac{b}{T(\text{K})} \tag{3}$$

for the solid. The results are summarized in Table 3. In addition to (2) and (3), a third form, i.e., $\ln P = a - b/T - c \ln T$, has been tried. Equation (2) gave significantly better results than the other two for the liquid, as exemplified by almost an order of magnitude better σ, while all functional forms yielded comparable results for the solid. The third column of Table 3, $\sigma(\log P)$, is the RMSD of the experimental points from (2) or (3). Thus, for liquid $^{14}NH_3$, the present work gives an average of 0.21% error in pressure, while the experimental points by Overstreet and Giauque [15] and Armstrong [1] respectively give 0.038% and 0.28% scatters relative to the values calculated using (2) and the corresponding parameters in Table 3. It is to be noted that Overstreet and Giauque used an ice point of their time, i.e., 273.10 K. The parameters given in the table have been obtained by re-fitting their experimental points after making the temperature correction. Armstrong's values are a result of his critical review of the then available data, including [15]. Armstrong's ice point was 273.16 K. As different as the parameters for NH_3 in Table 3 may look, the LSF equations derived from [1] and [15] yield numerical values of vapor pressure which agree with the present results within the stated limits of uncertainties in the specified temperature ranges.

Table 4. Triple points of isotopic ammonia.

Isotopic species	T_{tr}(K)		P_{tr}(torr)	
	Armstrong	This work	Armstrong	This work
$^{14}NH_3$	195.45	195.41	45.58	45.49
$^{14}ND_3$	199	198.96	48.22	48.35
$^{15}NH_3$	–	195.58	–	48.83

Armstrong's triple point temperatures [1] were based on the ice point of 273.16 K. The values in this table have been corrected.

Kiss, Matus, and Opauszky [17] reported (without experimental data) an equation, $T\log(P'/P) = 42.36 - 0.1244\,T$ for the H/D effect in the liquid, and $T\log(P'/P) = 105.4 - 0.4210\,T$ for the H/D effect in the solid. Their liquid equation gives values which are 1 to 3% lower than ours. The solid equation agrees well with ours in the immediate vicinity of the triple point of NH_3 but deviates increasingly at the lower temperatures (e.g., 16% higher than ours at $10^3/T$ of 6.0).

2) *Triple Points*

The triple points determined in the present study have been summarized in Table 4. That for NH_3 by Overstreet and Giauque [15] is 195.41 K (45.58 torr) after the 0.05 K correction, which is in good agreement with the present work. Armstrong's ND_3 triple

point is based on the results of Kirshenbaum and Urey [4].

It is worth pointing out that the difference in the vapor pressures of NH_3 and ND_3 does not change much at temperatures between the triple points of NH_3 and ND_3, while the magnitude of the vapor pressure changes considerably ($P' = 45.5$ torr ~ 60.4 torr) in the same range. This is illustrated in Fig. 4, in which a part of the experimental data set of Fig. 2 has been plotted differently at temperatures near the triple points of NH_3 and ND_3. The difference in the pressures in this range can be represented by

$$\delta P(\text{torr}) = P' - P = -(0.0251 \pm 0.0323)\, T(\text{K}) + (16.388 \pm 6.381),$$

with a RMSD of 0.181 torr in δP, meaning that δP is constant within the experimental uncertainties. The constancy of δP implies that the ratio of the heats of vaporization of liquid NH_3 ($\Delta H'_{\text{vap}}$) and sublimation of solid ND_3 (ΔH_{sub}) is equal to the ratio of the volume changes in the vaporization of NH_3 and the sublimation of ND_3, at any temperature within this range. Or, using the Clausius-Clapeyron equation, $P' \Delta H'_{\text{vap}} \approx P \Delta H_{\text{sub}}$ and $P'/P \approx \Delta S_{\text{sub}}/\Delta S'_{\text{vap}} > 1$. The least-squares fits of the individual vapor pressures to (3) in this range give

$$\frac{\Delta H\,(\text{sublimation})}{\Delta H'\,(\text{vaporization})} = \frac{7.724 \pm 0.019}{6.004 \pm 0.052} = 1.286 \pm 0.012$$

while the average of P'/P is 1.275. These observations appear to be valuable in elucidating the structure of liquid ammonia near its triple points. A further discussion of this subject is postponed for a future study.

3) *Reduced Partition Function Ratios*

The phase ratio of the reduced partition function ratios, f_c/f_g, has been calculated from the vapor pressure ratios, P'/P, by an application of the usual corrections [2, 9, 21],

$$\ln(f_c/f_g) = \left[1 + P'\left(B_o - \frac{V_c}{RT}\right)\right] \ln(P'/P) - \ln f^{g}_{\text{rot}}. \tag{4}$$

At temperatures between the triple points of two isotopic species we should add a third term, $-P\Delta V/RT$, where ΔV is the molar volume change on melting at T, to the right-hand side of (4) and, correspondingly, $V_c = V_{\text{liq}}$. This term, however, is negligible in the present case, e.g., -0.000009 at 196 K and -0.000012 at 199 K. The second virial coefficient $B_0(T)$ has been

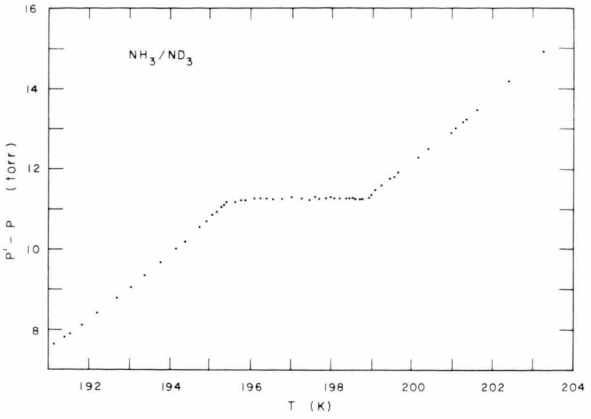

Fig. 4. Plot of $\delta P = P'(NH_3) - P(ND_3)$ vs. temperature near the triple points.

computed from

$$B_0(\text{torr}^{-1}) = -\frac{1625.80}{T^3} + \frac{6.577}{T^2} - \frac{7.427 \times 10^{-3}}{T}, \tag{5}$$

a formula which has been obtained by fitting the data given in [18] at temperatures between 200 K and 250 K. The molar volumes of the condensed phases have been calculated from

$$V_{\text{liq}}(\text{ml/mol}) = 1.258 \times 10^{-4}\, T^2 - 1.466 \times 10^{-2}\, T + 21.261 \tag{6}$$

and

$$V_{\text{sol}}(\text{ml/mol}) = 9.083 \times 10^{-3}\, T + 18.986, \tag{7}$$

both obtained by fitting the liquid (197.15 K – 239.15 K) and solid (81 K – 195.2 K) data from [18].

The contributions of the non-classical rotation in the gaseous molecules have been calculated for the symmetric top using the rotational constants obtained from the molecular geometry of Benedict and Plyler [19]: For $^{14}NH_3$: 9.99 cm^{-1} (expt'l = 9.94) and 6.35 cm^{-1} (expt'l = 6.31); for $^{14}ND_3$: 5.16 cm^{-1} (5.14) and 3.18 cm^{-1} (3.16); for $^{15}NH_3$: 9.96 cm^{-1} and 6.35 cm^{-1}. The experimental values indicated are from IR data [20]. No experimental data were available for $^{15}NH_3$. Thus,

$$\ln f^{g}_{\text{rot}} = -\frac{1.436}{T} - \frac{0.679}{T^2} \quad [\text{H/D}], \tag{8}$$

and

$$\ln f^{g}_{\text{rot}} = -\frac{3.12 \times 10^{-3}}{T} - \frac{2.21 \times 10^{-2}}{T^2} \quad [^{14}NH_3/^{15}NH_3]. \tag{9}$$

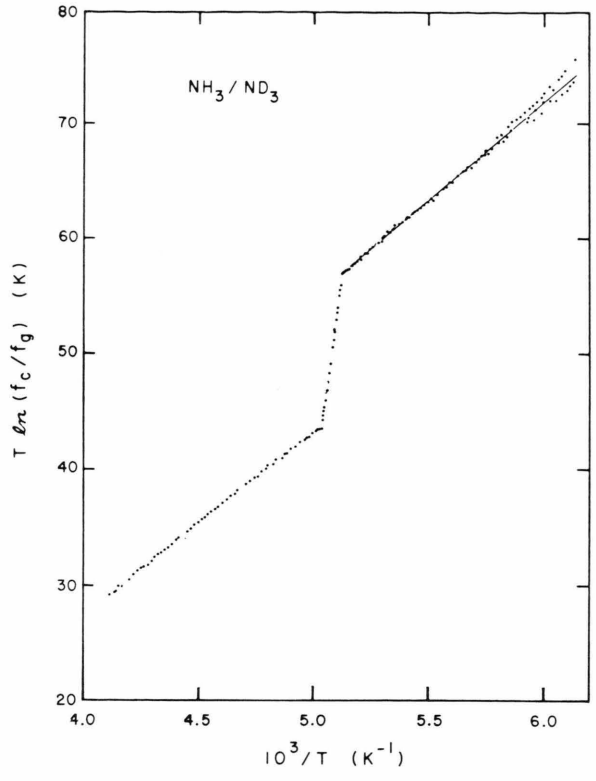

Fig. 5. Reduced partition function ratio for NH_3/ND_3. The solid line is calculated using the **F**-matrix of Table 7.

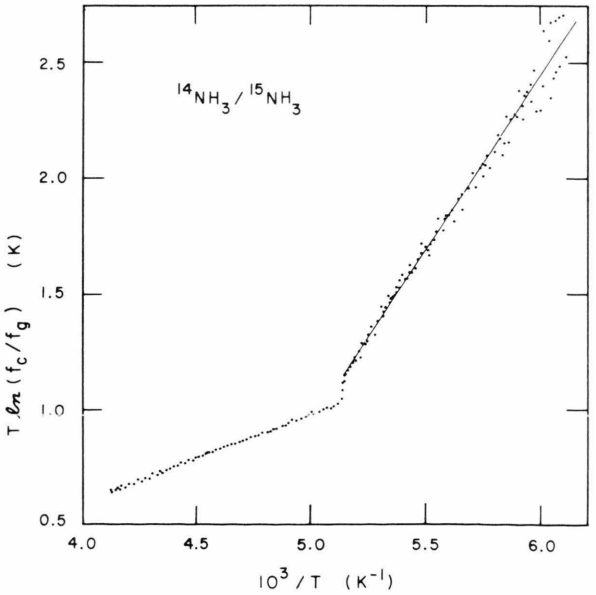

Fig. 6. Reduced partition function ratio for $^{14}NH_3/^{15}NH_3$. The solid line is calculated using the **F**-matrix of Table 7.

Table 5. Least-squares parameters for the reduced partition function ratios: Fit to eq. (10).

Isotopic pair	Condensed phases	A	B
NH_3/ND_3	liquid/liquid	15793 ± 46	35.62 ± 0.21
	liquid/solid	145070 ± 19	685.6 ± 9.8
	solid/solid	17070 ± 105	30.35 ± 0.59
$^{14}NH_3/$ $^{15}NH_3$	liquid/liquid	372.2 ± 2.2	0.8776 ± 0.0101
	liquid/solid	27600 ± 21	140 ± 11
	solid/solid	1476 ± 16	6.4058 ± 0.0936

The non-classical contributions to the H/D effect are relatively more significant (e.g., -0.0059 and -0.0088 at 243 K and 163 K, respectively) than those for the 14/15 effect (e.g., -1.34×10^{-5} at 240 K and -2.00×10^{-5} at 163 K).

The phase ratios of the reduced partition function ratios, f_c/f_g, thus calculated are plotted in Figs. 5 and 6. The straight lines are in the form

$$T \ln (f_c/f_g) = \frac{A}{T} - B, \tag{10}$$

the coefficients A and B being tabulated in Table 5.

Although both H/D and $^{14}N/^{15}N$ VPIEs are normal, i.e., the lighter molecule exhibits the higher vapor pressure, the effect of the d_3-for-d_0 substitution is greater than that of the ^{15}N-for-^{14}N substitution by more than an order of magnitude. This indicates significant hindrance of librational motions of ammonia molecules in its condensed phases.

4) Molecular Forces in the Condensed Ammonia

The method of vapor pressure isotope effect pioneered by Bigeleisen is one of the most powerful tools for elucidation of the forces acting on the molecules in condensed phases, as Bigeleisen [21] and many who followed him (notably, Van Hook, Wolfsberg, and their associates) have illustrated by excellent examples. The usefulness of the VPIE method is based on the fact that it directly gives information on the mean second derivatives of the potential energy felt by the condensed phase molecules. Technically, the forces in the condensed phases are found by calculating f_c (i.e., f_{solid} or f_{liq}) from f_c/f_g and f_g, the latter being computed mainly from spectroscopic information, and then theorizing on the structure and forces in the condensed phase using a structural model. One usually assumes validity of the Born-Oppenheimer approxi-

mation and try to reproduce not only the observed VPIEs but also other isotopic properties such as the spectroscopic data in the condensed phase using a single force constant matrix per phase.

The Gas

Ŝpirko's anharmonic potential function [22] reproduces well all known experimental frequencies of gaseous NH_3, ND_3 and $^{15}NH_3$, including the doublets resulting from the umbrella-type inversion of the pyramidal molecule. We used the frequencies calculated (Table 6) from his force constants to compute the reduced partition function ratios (RPFRs) of the gas phase, $f_g(d_0/d_3)$ and $f_g(14/15)$, as the square roots of the f obtained from

$$\ln(s/s')f = \sum_i \delta \ln b(u_i), \tag{11}$$

where the summation was taken over the twelve split frequencies for the gas and

$$\ln b(u_i) = \frac{u_i}{2} - \ln u_i + \ln(1 - e^{-u_i}), \tag{12}$$

$$\delta \ln b(u_i) = \ln b(u_i') - \ln b(u_i), \tag{13}$$

$$u_i = h c \nu_i / kT. \tag{14}$$

Table 6. Fundamentals and calculated frequencies of gaseous ammonia. Benedict [19], Ŝpirko [22], Morgan [23].

Molecule	Mode	Exp. (cm^{-1})	Calc. (cm^{-1})
		Benedict	Ŝpirko
NH_3	$\nu_1(A_1)$	3336.2	3342.0
		3337.2	3343.4
	$\nu_2(A_1)$	932.5	930.4
		968.3	968.8
	$\nu_3(E)$	3443.6	3455.9
		3443.9	3456.7
	$\nu_4(E)$	1626.1	1631.3
		1627.4	1631.8
ND_3	$\nu_1(A_1)$	2420.1	2428.8
		2420.6	2429.4
	$\nu_2(A_1)$	745.7	745.3
		749.4	749.2
	$\nu_3(E)$	2564.0	2576.1
			2576.2
	$\nu_4(E)$	1191.0	1182.3
			1182.4
		Morgan	
$^{15}NH_3$	$\nu_1(A_1)$	3335	3338.2
			3339.7
	$\nu_2(A_1)$	926.3	926.7
		961.0	963.8
	$\nu_3(E)$	—	3446.3
			3447.1
	$\nu_4(E)$	1625.0	1628.6
			1629.0

The Solid

Neutron diffraction [24, 25] and x-ray diffraction [26] studies of crystalline ammonia-d_0 and ammonia-d_3 agree about the solid being of the cubic space group, $P_{2_13}(T^4)$, with four molecules per unit cell on the sites of C_3 symmetry. Each molecule is hydrogen-bonded to six nearest neighbors, three as a proton-donor and three through hydrogen atoms from three other neighbors.

Our goal here was to develop an **F**-matrix for the solid ammonia which best reproduces the present VPIE data, namely f_s/f_g as a function of temperature for both isotopic pairs and also all available spectroscopic data of isotopic solid ammonias. The infrared and Raman spectra of crystalline ammonia have been studied by a number of groups [27]. We chose to fit our solid **F**-matrix to the results of Binbrek and Anderson [27 b] for the internal consistency of their data. It is the most extensive spectroscopic study of the isotopic frequencies of vibrational and lattice modes in the IR and Raman at temperatures ranging between 18 K and 107 K. Their data generally agree well with other group's. We used a unit cell model consisting of four molecules to represent our solid and treated the cluster by means of the **FG** matrix method in the following manner.

The unit cell used is that of Reed and Harris [24] which may be qualitatively described as follows. If one places one of the four molecules on a corner of a cubic lattice with the N→H vectors directing outward from the cube (and symmetrically placed around an extension of the main diagonal of the cube), three other molecules are almost on the facecenters of the three mutually perpendicular faces of the cube that intersect each other at the first corner. One of the N→H vectors on each of the face molecules points almost directly to the nitrogen of the corner molecule. Within each molecule R(N–H) = 1.005 Å and H–N–H angle = 110.4°. The unit cell dimensions are 5.073 Å for ND_3 and 5.084 Å for NH_3 [24, 26]. The equilibrium positions of the 16 atoms were set up accordingly.

We completely neglected the kinetic energy coupling terms among the 4 molecules: A 48 × 48 **G**-matrix of the cluster was set up without defining any coordinate which would have explicitly involved simultaneous motions of atoms belonging to different

Table 7. **F**-matrix of solid ammonia in valence coordinates *.

Description	Notation	Value (mdyn Å^{-1} or mdyn Å)
N^c–H stretch	f_D	5.835
N^f–H stretch	f_d	5.834
HN^cH bend	f_α	0.569
HN^fH bend	f_β	0.569
Str^c–Str^c interact	f_{DD}	−0.041
Str^f–Str^f	f_{dd}	−0.041
$Bend^c$–$Bend^c$	$f_{\alpha\alpha}$	−0.0040
$Bend^f$–$Bend^f$	$f_{\beta\beta}$	−0.0041
Str^c–$Bend^c$	$f'_{D\alpha}$	0.046
Str^c–$Bend^c$	$f_{D\alpha}$	−0.0426
Str^f–$Bend^f$	$f'_{d\beta}$	0.046
Str^f–$Bend^f$	$f_{d\beta}$	−0.0426
Translation	$f^c_{T_z}$	$0.158-(1.8061\times10^{-3})\Delta+(8.7505\times10^{-6})\Delta^2$
	$f^c_{T_{xy}}$	$0.1154-(7.4132\times10^{-4})\Delta$
	$f^f_{T_z}$	$0.3360-(3.4349\times10^{-3})\Delta+(1.5771\times10^{-4})\Delta^2$
	$f^f_{T_{xy}}$	$0.1012-(5.2011\times10^{-4})\Delta$
Rotation	$f^c_{R_z}$	$0.1558-(5.1828\times10^{-4})\Delta$
	$f^c_{R_{xy}}$	$8.5272\times10^{-2}-(2.5960\times10^{-4})\Delta$
	$f^f_{R_z}$	$1.0989\times10^{-1}-(3.3455\times10^{-4})\Delta$
	$f^f_{R_{xy}}$	$0.2054-(6.6728\times10^{-4})\Delta$
Ext–Ext	$f^f_{T_x-T_y}$	$9.9600\times10^{-2}-(4.4630\times10^{-4})\Delta+(7.4074\times10^{-6})\Delta^2$
	$f^f_{R_x-R_y}$	$6.5534\times10^{-2}-(2.5868\times10^{-4})\Delta$
Int–Ext	$f^c_{\alpha-T_z}$	$-1.000\times10^{-3}-(4.1183\times10^{-3})\Delta-(8.4982\times10^{-5})\Delta^2$
	$f^f_{\beta-T_z}$	$1.000\times10^{-3}+(4.0429\times10^{-3})\Delta-(2.5714\times10^{-4})\Delta^2$
	$f^c_{D-T_z}$	$(5.8181\times10^{-3})\Delta+(2.6252\times10^{-4})\Delta^2$
	$f^f_{\beta-T_z}$	$(-1.0315\times10^{-2})\Delta-(6.8580\times10^{-4})\Delta^2$

* All elements are in units of mdyn Å^{-1}, except f_R's and the interactions among f_R's, which are in units of mdyn Å. $\Delta = T(K)-180$. The superscripts, c and f, denote the corner and face molecules, respectively. The primed f (e.g., $f'_{D\alpha}$) refers to an interaction between an NH stretch and an HNH bend in which the nitrogen atom is the only atom shared by the two coordinates, while the unprimed f (e.g., $f_{D\alpha}$) refers to the one between the two coordinates in which an N–H bond is shared. For the external modes, the molecular symmetry axis is the z-axis. The notation such as $f_{T_{xy}}$ means that the element applies to the translation in the molecular xy-plane, while $f_{T_x-T_y}$ refers to an interaction between the coordinates T_x and T_y.

molecules in the cluster. Thus in this model the intermolecular interactions were accounted for solely through off-diagonal terms in the corresponding **F**-matrix. The coordinate system was set up as follows; 24 valence coordinates (three N–H stretching and three H–N–H angle-bending coordinates per molecule) and 24 intermolecular coordinates (six orthonormal coordinates [28] per molecule for the local external modes). Three of the latter 24 correspond to the acoustic modes. All bending coordinates were weighted by the equilibrium distance of the N–H bond, which is 1.005 Å. Assignments of the calculated normal frequencies were made on the basis of the magnitudes and symmetries of the elements of vibrational eigenvectors.

A procedure based on the method of derivatives [11] has led to the final **F**-matrix for the solid, which is summarized in Table 7. In the method a matrix of first derivatives of frequencies and several representative values of VPIEs with respect to the elements of an **F**-matrix are computed for every isotopic molecule, and desired adjustments in the frequencies and VPIEs are obtained as a linear combination of the elements of the derivative matrix. The **F**-matrix resulting from this step constitutes an improved **F**-matrix, which is then used as a basis of the next round of **F**-matrix fitting. After every round the magnitudes of the new **F**-matrix elements and their shifts from the gas **F**-matrix are checked for reasonableness, and discretionary adjustments are made where they are justified.

The vibrational and lattice frequencies calculated from the **F**-matrix of Table 7 thus obtained are compared with the observed fundamentals [27 b] in Tables 8 and 9, respectively. Table 9 also lists the results from a lattice dynamics study by Righini [29]. The agreement is satisfactory.

The RPFR of the solid, f_s, has been computed as the quartic root of the f obtained by taking the summation in (11)–(14) over the 48 normal frequencies corresponding to this **F**-matrix. The solid lines through the solid/solid temperatures in Figs. 5 and 6 have been drawn according to thus calculated f_s/f_g. The agreement is excellent.

The Liquid

Compared to crystalline ammonia, not much is experimentally known about the structure of liquid ammonia. The x-ray diffraction study by Kruh and Petz [30] showed that, in the liquid at 199, 228 and 277 K,

Table 8. Fundamentals and calculated frequencies (cm^{-1}) of solid ammonia. Anderson [27 b].

Molecule	Mode	Experimental Anderson (107 K)	Calculated This work (180 K)
NH_3	ν_1 (A)	3210	3146
	ν_2 (A)	1058	1019
	ν_3 (E)	3370	3292
	ν_4 (E)	1650	1621
ND_3	ν_1 (A)	2335	2246
	ν_2 (A)	814	775
	ν_3 (E)	2505	2431
	ν_4 (E)	1196	1179
$^{15}NH_3$	ν_1 (A)	–	3144
	ν_2 (A)	–	1014
	ν_3 (E)	–	3283
	ν_4 (E)	–	1618

each ammonia molecule is surrounded on the average by about 11 neighbors, 7 at a mean distance of 3.56 Å and 4 at 4.1 Å. Narten's x-ray study [31] at 277 K gave a first peak in the radial distribution function of N–N at a distance of 3.4 Å and a pronounced shoulder at 3.7 Å. No experimentally observed lattice frequencies have been reported, except for a broad, weak band centered around 320 cm^{-1} observed by Lemley et al. [32].

We have analyzed the present VPIE data for the liquid by using a simple cell model. The molecular geometry of the gas molecule [19] was used for the liquid molecules. The coordinates consisted of three N–H stretches, three HNH bends (weighted by the equilibrium N–H distance of 1.0124 Å), and three translational and three librational coordinates. The **F**-matrix was determined by mainly fitting the internal block to the fundamentals reported by Lemley [32] and the external block to the magnitudes and slopes of the plots of $T\ln(f_l/f_g)$ vs. $1/T$ (Figs. 5 and 6) in the liquid/liquid temperature range for both VPIEs. The final liquid **F**-matrix and the frequencies calculated from it are presented in Tables 10 and 11, respectively. This **F**-matrix, which consists of only 10 distinct elements, reproduces the experimental points in the liquid/liquid range in Figs. 5 and 6 so closely that for the sake of clarity no calculated lines have been added to the Figs. 5 and 6.

For both VPIEs the combination of the **F**-matrices of the solid (Table 7) and liquid (Table 10) also gives excellent agreements with experiment at temperatures between the triple points. No lines have been drawn in this range in Figs. 5 and 6 to avoid obscuring the data points.

Table 9. Comparison of lattice frequencies of solid ammonia.

Molecule	Mode	Exp. (cm^{-1})	Calculated (cm^{-1})	
		Anderson (80 K)	Righini	This work (180 K)
NH_3	A ν_1 T_z	–	144	126
	ν_2 R_z	310	306	311
	E ν_3 T_{xy}	107	122	107
	ν_4 R_{xy}	298	299	298
	F ν_5 T_{xyz}	140	130 TO 132 LO	141
	ν_6 T_{xyz}	183	181	183
	ν_7 R_z	260	273 TO 274 LO	260
	ν_8 R_{xy}	426 TO 358 LO 358	423 360 360	381 381 381
	ν_9 R_{xy}	533	524 TO 530 LO	532
ND_3	A ν_1 T_z	–	131	116
	ν_2 R_z	242	223	220
	E ν_3 T_{xy}	100	113	99
	ν_4 R_{xy}	227	219	214
	F ν_5 T_{xyz}	129	122 TO 124 LO	130
	ν_6 T_{xyz}	173	168	168
	ν_7 R_z	192	196	184
	ν_8 R_{xy}	315 267 267	306 262 262	273 273 273
	ν_9 R_{xy}	406	383 TO 388 LO	381
$^{15}NH_3$	A ν_1 T_z			122
	ν_2 R_z			311
	E ν_3 T_{xy}			104
	ν_4 R_{xy}			298
	F ν_5 T_{xyz}			137
	ν_6 T_{xyz}			178
	ν_7 R_z			260
	ν_8 R_{xy}			381 381 381
	ν_9 R_{xy}			532

LO and TO are the longitudinal and transverse components of Raman spectra, respectively. Anderson [27 b], Righini [29]. Values of this work computed using **F**-matrix of Table 7.

5) An Overview

Earlier in this paper we have noted the contrasting difference in the magnitudes of VPIEs between the H/D and 14/15 substitutions. We further note that the slopes in the H/D-VPIE plots (Figs. 2 and 5) increase only mildly in going from the liquid/liquid to the solid/solid range, while the ones in the 14/15-VPIE plots (Figs. 3 and 6) increase by a factor of about 4 between the liquid/liquid and solid/solid ranges. In the following we offer an explanation for these experimental facts.

Table 10. **F**-matrix of liquid ammonia in valence coordinates.

Description	Notation	Value (mdyn Å^{-1} or mdyn Å)
N–H stretch	f_r	6.015
HNH bend	f_α	0.529
	f_{rr}	−0.003
	$f_{\alpha\alpha}$	−0.049
	$f_{r\alpha}$	−0.0416
	$f_{r'\alpha}$	0.044
Translation	f_T	$f_{trans} = 0.1421 - 3.4177 \times 10^{-4}\,\Delta$
Rotation	f_R	$f_{rot} = 0.1040 - 8.6319 \times 10^{-5}\,\Delta + 1.8428 \times 10^{-6}\,\Delta^2$
Internal-External	f_{DT_z}	+0.0268
Interaction	$f_{\alpha T_z}$	+0.0042

All elements are in units of mdyn Å^{-1} except f_R's which are in units of mdyn Å. $\Delta \equiv T - 217$.

Table 11. Vibrational and external frequencies (cm^{-1}) for liquid ammonia.

Mode	$^{14}NH_3$			$^{14}ND_3$			$^{15}NH_3$
	Lemley	Birchall	Calc.	Lemley	Birchall	Calc.	Calc.
$\nu_1(A_1)$	3300	3240	3229	2403	2344	2318	3226
$\nu_2(A_1)$	1046	1066	1012	809	816	765	1007
$\nu_3(E)$	3385	3379	3325	2521	2517	2450	3316
$\nu_4(E)$	1638	1638	1578	1198	1203	1144	1575
T_{xyz}	—	—	119	—	—	109	116
R_{xy}	320	—	323	—	—	232	323
R_z	—	—	258	—	—	182	258

Lemley [32], Birchall [33]. Calculated is this work using the liquid **F**-matrix at 217 K.

Table 12. Comparison of various contributions to $T \ln (f_c/f_g)$ in isotopic ammonias. All values in K.

	$T \ln (f_s/f_g)$ at 195.41 K		$T \ln (f_l/f_g)$ at 198.98 K	
	d_0/d_3	14/15	d_0/d_3	14/15
Translations	3.0	6.07	2.6	1.68
Rotations	84.4	1.48	76.7	0.19
Internal vibrations	−31.9	−6.41	−37.1	−0.88
Non-classical rotations	1.5	0.0	1.5	0.0
Total	57.0	1.14	43.8	0.99

Although numerically not unique, we have found the temperature-dependencies of the intermolecular elements in the condensed phase **F**-matrices (Tables 7 and 10) essential in order to reproduce the experimentally observed VPIEs and the spectroscopic data. It has been especially so for the solid **F**-matrix to yield the relatively large slope of the 14/15-plot in that phase. The temperature coefficients of rotational force constants for the solid (see, for instance, the term $-5.1828 \times 10^{-4}\,\Delta$ in $f^c_{R_2}$; $\Delta \equiv T(\mathrm{K}) - 180$) are an order of magnitude higher than those for the liquid (e.g., the term $-8.6319 \times 10^{-5}\,\Delta$ for f_R; $\Delta = T(\mathrm{K}) - 217$). The temperature coefficients of the force constants of translational motions of solid molecules in the direction of the molecular symmetry axis (f_{T_z}) are much greater (by a factor of 2.5 to 6) than those for translations in the directions perpendicular to the axis. These are the necessary consequences of the four-fold change in the slopes of the 14/15-plot between the liquid and solid ranges. What this physically means is that the intermolecular forces hindering the external molecular motions, especially the librations, in the solid become stronger and rapidly anisotropic with decreasing temperature in the solid range that we have investigated.

Table 12 illustrates the magnitudes of contributions of various molecular motions to $T \ln (f_s/f_g)$, computed from the **F**-matrices obtained in this work and using (11)–(14), with the appropriate factoring to give proper accounts of per-molecule contributions in both condensed phases. In terms of the approximation (10), the translational and librational contributions to $\ln (f_c/f_g)$ comprise the first quantum correction term of A/T^2, while the isotopic difference in the shifts of zero-point energy upon condensation of gaseous molecule and the non-classical rotations constitute $-B/T$. Thus, the slopes in Figs. 5 and 6 are primarily determined by the translational and rotational contributions, while the ordinates have important contributions from all molecular motions.

It is seen from Table 12 that the rotational contribution does in fact determine most of the difference in the H/D and 14/15 VPIE. This makes it clear that the rotational motions of ammonia in the liquid are hindered. The large differences in the rotational contributions between the H/D and 14/15 substitutions (Table 12) are due to the fact that the off-the-axis substitutions in d_0/d_3 cause large changes in all rotational constants, while the ^{14}N-for-^{15}N substitution is on the axis of symmetry and near the center of the molecular mass, so that the hindered rotations affect the isotopic difference only insignificantly.

Furthermore, we conclude from Table 12 that the relatively small change in the slopes of the H/D-plots between the liquid and solid (Fig. 2) must be due to the hindrance of rotation in the liquid being about the

same as in the solid, as far as the motions of hydrogen atoms are concerned. In contrast, the rotational contribution on nitrogen substitution changes distinctively from 0.19 K to 1.48 K in Table 12 (Fig. 3), although they are small in magnitudes compared to those of the hydrogen isotope effect. This suggests a significant difference between liquid and solid forces resisting movement of the nitrogen atom in the directions perpendicular to the molecular figure axis.

Table 12 illustrates that the large change in the slopes of the 14/15-VPIE plot is due to the changes in the translational modes. The Table also shows a high level of interaction between the internal and external modes, especially in the solid. In the absence of such interactions the contribution of translational modes for the d_3-for-d_0 substitution should have been greater than that for the ^{15}N-for-^{14}N substitution. This is not the case in the solid ammonia. The large translational contribution to 14/15-VPIE in the solid is attributable to a high degree of translational-vibrational interactions associated with nitrogen motion in the solid. The change in the translational contributions is balanced by a shift in the zero-point energy effects which is of similar magnitude as that of the translational effects but of opposite sign. In contrast, the motions of hydrogen atoms which would influence both translation and libration appear to be not much different in the liquid and the solid; this would explain the small increases in the contributions (Table 12) of translation and rotation to the H/D-VPIE upon solidification.

The schematic picture which emerges from these observations is that the rotation of ammonia molecules in the liquid is strongly hindered principally because of external forces acting against the rotational motion of hydrogen and not as much because of the forces acting against nitrogen motion. Let us at this point compare this picture with some other experimental facts and theoretical results.

The x-ray studies on the liquid at temperatures ranging from 199 to 277 K showed 11 [26] or 12 [31] nearest neighbors at distances ranging from 3.5 Å to 4.1 Å, while the neutron diffraction experiments on the solid at 77 K [24] gave 12 nearest neighbors, i.e., 3 at 3.35 Å and 3 at 3.88 Å. Except for the thermal expansion and thermal disturbances in the liquid, the more or less close-packed structure apparently persists not only through the phase change but also over a wide temperature range in the liquid.

Our recent molecular dynamics study based on a newly developed, flexible, four-site model of liquid ammonia [34] also confirmed the coordination number of 12 at 235 K and 277 K, with a slightly more pronounced first neighbor structure at the lower temperature. All other MD and MC studies also reported coordination numbers ranging from 12 to 13 [35]. The result that the effective coordination number and the nearest neighbor distances are relatively insensitive to the change in temperature is consistent with the present observation that the hindrance against rotation is fairly well developed in the liquid. On the lone-pair side of nitrogen, the depth of the potential minimum varies only slowly with the changes in the azimuthal and polar directions of the proton-donating N–H bonds of the nearest neighbors as viewed from the proton-accepting molecule [34]. Thus, in the liquid, there seem to be little directional forces on the lone-pair side of the nitrogen, while the hydrogens on the other side of the molecule are tied down by the nitrogens of approximately three nearest neighbor molecules, although very weakly. This, from the viewpoint of the present discussion, may be responsible for the rotational hindrance: The weak directionality of the external forces on the hydrogen side of the molecule may be sufficient to yield the significant difference in the rotational effects for the H/D-VPIE, while the practical absence of similar directionality on the lone-pair side of the liquid ammonia molecule explains the small rotational contributions in the nitrogen isotope effect.

The MD results are thus consistent with the observation for the liquid. In the solid, the molecules on the lone-pair side start to fall into their places rapidly with decreasing temperature, thus creating the more directional intermolecular forces on the nitrogens atoms. This seems to be the reason for the distinct increase in the slopes observed in the present ^{14}N/^{15}N-VPIE plots.

IV. Conclusion

The H/D- and ^{14}N/^{15}N-vapor pressure isotope effects in liquid and solid ammonia can be satisfactorily interpreted on the basis of the theory of isotope effects in condensed phases originally founded by Professor Jacob Bigeleisen, to whom this paper is dedicated. A 4-molecule unit cell model and a simple cell model adequately describe the solid and liquid ammonia, respectively.

Within the temperature range studied, both VPIEs in both condensed phases are best described in terms

of the two-term approximation, one term being the first quantum correction due to intermolecular motions and another which mainly consists of the isotopic difference in the shifts of the vibrational zero-point energy upon condensation of gaseous molecules. The first quantum corrections for the H/D-VPIE in both solid and liquid are dominated by those due to hindered rotations. Rotation in the liquid is significantly hindered, which seems to be due to the external forces acting against such molecular rocking effects caused by motions of hydrogen atoms (rather than those of nitrogen atoms) in the ammonia molecules in the liquid. The observed 4-fold increase in the slopes of the $T\ln(P'/P)$ vs. $1/T$ plot and $T\ln(f_c/f_g)$ vs. $1/T$ plot, going from the liquid/liquid to solid/solid range, can be explained as a combined effect of i) significant temperature-dependencies in the interactions in the solid between internal vibrational modes and the translational motions in the direction of the molecular axis, ii) a high directionality of external forces acting on the nitrogen atom in the solid, and iii) the absence of such directionality in the liquid phase.

It is noted that the difference in the vapor pressures of NH_3 and ND_3 is, within our experimental errors, independent of temperature changes in the range between the triple points of these isotopic molecules.

Acknowledgements

This research was supported by the Division of Chemical Sciences, Office of Basic Energy Sciences, U.S. Department of Energy, under Grant No. DE-FG02-88ER13855.

[1] G. T. Armstrong, Natl. Bur. Standards Report No. 2626, June, 1953.
[2] G. Jancsó and W. A. Van Hook, Chem. Rev. **74,** 691 (1974).
[3] H. S. Taylor and J. C. Jungers, J. Amer. Chem. Soc. **55,** 5057 (1933); J. Chem. Phys. **2,** 373 (1934).
[4] I. Kirshenbaum and H. C. Urey, J. Chem. Phys. **10,** 706 (1942).
[5] H. Wolff and A. Höpfner, Ber. Bunsenges. Phys. Chem. **73,** 480 (1969).
[6] W. Groth, H. Ihle, and A. Murrenhoff, Angew. Chem. **68,** 605 (1956).
[7] H. G. Thode, J. Amer. Chem. Soc. **62,** 581 (1940).
[8] J. Bigeleisen, F. P. Brooks, T. Ishida, and S. V. Ribnikar, Rev. Sci. Instrum. **39,** 352 (1968).
[9] J. Bigeleisen, J. Chem. Phys. **34,** 1485 (1961).
[10] M. J. Stern, W. A. Van Hook, and M. Wolfsberg, J. Chem. Phys. **39,** 3179 (1963).
[11] A. Popowicz, T. Oi, J. Shulman, and T. Ishida, J. Phys. Chem. **76,** 3732 (1982).
[12] T. Oi, J. Shulman, A. Popowicz, and T. Ishida, J. Phys. Chem. **87,** 3153 (1983).
[13] A. Kanungo, T. Oi, A. Popowicz, and T. Ishida, J. Phys. Chem. **91,** 4198 (1987).
[14] J. Bigeleisen, J. Chem. Phys. **23,** 2264 (1955); ibid. **28,** 694 (1958).
[15] R. Overstreet and W. F. Giauque, J. Amer. Chem. Soc. **59,** 254 (1937).
[16] (a) E. C. McKelvey and C. S. Taylor, Sci. Papers, Bur. Standards **18,** 655 (1923); (b) F. W. Bergstrom, J. Phys. Chem. **26,** 359 (1922); (c) F. Henning and A. Stock, Z. Physik **4,** 226 (1921); (d) C. S. Cragoe, C. H. Meyers, and C. S. Taylor, Sci. Papers, Bur. Standards No. 369, **16,** 1 (1920); (e) S. Postma, Rec. Trav. Chim. **39,** 515 (1920); (f) E. Karwat, Z. physik. Chem. **112,** 486 (1924).
[17] I. Kiss, L. Matus, and I. Opauszkey, Kernenergie **5,** 329 (1962).
[18] L. Haar and J. S. Gallagher, J. Phys. Chem. Ref. Data **7,** 635 (1978).
[19] W. S. Benedict and E. K. Plyler, Can. J. Phys. **35,** 1235 (1957).
[20] G. Herzberg, Molecular Spectra and Molecular Structure. II. Infrared and Raman Spectra of Polyatomic Molecules, Van Nostrand Reinhold Co., Princeton, New Jersey, 1945.
[21] For example: J. Bigeleisen, S. V. Ribnikar, and W. A. Van Hook, J. Chem. Phys. **38,** 489 (1963); J. Bigeleisen, C. B. Cragg, and M. Jeevanandam, ibid. **47,** 4335 (1967); J. Bigeleisen, M. W. Lee, and F. Mandel, Acct. Chem. Res. **8,** 179 (1975); Y. Yato, M. W. Lee, and J. Bigeleisen, J. Chem. Phys. **63,** 1555 (1975); Z. Bilkadi, M. W. Lee, and J. Bigeleisen, ibid. **62,** 2087 (1975); J. Bigeleisen, S. Fuks, S. V. Ribnikar, and Y. Yato, ibid. **66,** 1689 (1977).
[22] V. Špirko, J. Mol. Spectrosc. **101,** 30 (1983).
[23] M. Morgan, P. Staats, and J. Goldstein, J. Chem. Phys. **27,** 1212 (1957).
[24] J. Reed and P. Harris, J. Chem. Phys. **35,** 1730 (1961).
[25] A. Hewat and C. Riekel, Acta Cryst. **A 35,** 569 (1979).
[26] I. Olovsson and D. Templeton, Acta Cryst. **12,** 832 (1959).
[27] (a) A. Bromberg, S. Kimel, and A. Ron, Chem. Phys. Lett. **46,** 262 (1977); (b) O. Binbrek and A. Anderson, ibid. **15,** 241 (1972); (c) H. Wolff, H. G. Rollar, and E. Wolff, J. Chem. Phys. **55,** 1373 (1971); (d) J. Corset, P. Huong, and J. Lascombe, Spectrochim. Acta **24 A,** 1385 (1968); (e) F. Reding, and D. Hornig, J. Chem. Phys. **22,** 1926 (1954); ibid. **19,** 594 (1951).
[28] E. B. Wilson, Jr., J. C. Decius, and P. C. Cross, Molecular Vibrations, McGraw-Hill Book Co., New York 1955.
[29] R. Righini, N. Neto, S. Califano, and S. H. Walmsley, Chem. Phys. **33,** 345 (1978).
[30] R. Kruh and J. Petz, J. Chem. Phys. **41,** 890 (1964).
[31] A. H. Narten, J. Chem. Phys. **66,** 3117 (1977).
[32] A. Lemley, J. Roberts, K. Plowman, and J. Lagowski, J. Phys. Chem. **77,** 2185 (1973).
[33] T. Birchall and I. Drummond, J. Chem. Soc. **A 1970,** 1859.
[34] S. V. Hannongbua, T. Ishida, E. Spohr, and K. Heinzinger, Z. Naturforsch. **43 a,** 572 (1988).
[35] A. Hinchliff, D. G. Bounds, M. L. Klein, I. R. McDonald, and R. Righini, J. Chem. Phys. **74,** 1211 (1981); (b) R. W. Impey and M. L. Klein, Chem. Phys. Lett. **104,** 579 (1984); (c) M. L. Klein, I. R. McDonald, and R. Righini, J. Chem. Phys. **71,** 3673 (1979).